Connection between topological pumping effect and chiral anomaly in Weyl semimetals

Ming-Xun Deng [1,2,*] Ya-Chen Hu,[1] Wei Luo [3] Hou-Jian Duan,[1,2] and Rui-Qiang Wang[1,2,†]

[1]*Guangdong Provincial Key Laboratory of Quantum Engineering and Quantum Materials, School of Physics and Telecommunication Engineering, South China Normal University, Guangzhou 510006, China*
[2]*Guangdong-Hong Kong Joint Laboratory of Quantum Matter, South China Normal University, Guangzhou 510006, China*
[3]*School of Science, Jiangxi University of Science and Technology, Ganzhou 341000, China*

While the semiclassical Boltzmann approach has been widely adopted to study chiral-anomaly-related transport in Weyl semimetals (WSMs), it predicts an unphysical diverging electrical conductivity when $E_F \to 0$, where E_F is the Fermi energy. Here, we develop a modified semiclassical equation of motion which includes both the diagonal and off-diagonal contributions of the Berry curvature. On this basis, we derive an undivergent classical formula for the positive longitudinal magnetoconductivity in a WSM which resolves the conflict between the classical and ultraquantum approaches. We demonstrate that the chiral anomaly is closely related to the topological pumping effect and it can be realized even in the absence of a magnetic field. With our findings we propose a different perspective to understand the topological properties of WSMs and suggest a way to measure the chiral anomaly using transport.

I. INTRODUCTION

In the past few years, considerable attention has been paid to topological phases of matter, ranging from gapped topological insulators to various gapless topological semimetals [1–10]. Weyl semimetals (WSMs), a typical example of three-dimensional topological semimetals, have been widely studied on both the theoretical [11–35] and experimental [36–50] sides. A WSM possesses linear-dispersion excitations near the degenerate band touching points, referred to as Weyl nodes, around which the Berry flux enclosed by the Fermi surface is quantized. The Weyl nodes can be understood as topological charges of definite chirality, acting as the source or sink of the Berry curvature in momentum space [51–53].

Soon after the theoretical predictions [54,55], the WSM state was experimentally found in TaAs [38–40] and later in several different compounds [56–60]. Their peculiar topological properties endow WSMs with multiple interesting physics. The most prominent ones are the chiral anomaly and chiral magnetic effect (CME). In the context of topological field theory, the CME and chiral anomaly in WSMs can be observed when the paired Weyl nodes are separated in energy-momentum space by a nodal separation four-vector $(b_0, \boldsymbol{b})$. While the four-vector does not break the chiral symmetry of the action, it breaks the system's Lorentz symmetry [61]. Consequently, as the four-vector is eliminated by a series of infinitesimal chiral transformations, a Chern-Simons-like term from the path integral measure will be introduced [61–64] and then results in the anomalous electromagnetic response $\boldsymbol{j} = \frac{e^2}{2\pi^2\hbar}(b_0\boldsymbol{B} + \boldsymbol{b} \times \boldsymbol{E})$. The gauge invariance of the

system will lead to the continuity equation

$$\partial_\nu j_5^\nu = \frac{e^2}{2\pi^2\hbar^2}\boldsymbol{E} \cdot \boldsymbol{B}, \qquad (1)$$

with $j_5^{\nu \geqslant 1}$ (j_5^0) being the chiral current (charge) density and $\boldsymbol{E}$ and $\boldsymbol{B}$ being external electric and magnetic fields. The chiral anomaly described by Eq. (1) indicates the violation of the number conservation laws of the chiral charge when $\boldsymbol{E} \cdot \boldsymbol{B} \neq 0$, which creates a charge imbalance between the two opposite Weyl nodes, leading to the so-called chiral chemical potential. The CME $\boldsymbol{j} \sim b_0\boldsymbol{B}$ indicates that the measurable charge current can be triggered by a magnetic field if the Weyl nodes are separated in energy or the chiral chemical potential exists.

In the semiclassical perspective, the emerging anomalous phenomena in WSMs are attributable to the Berry curvature in the quasiclassical equations of motion (EOMs) [65]. Together with the Boltzmann equation, one can derive a term $\propto(\boldsymbol{E} \cdot \boldsymbol{B})\boldsymbol{B}/E_F^2$ in the charge current density, which is interpreted as the chiral-anomaly-related positive longitudinal magnetoconductivity (LMC) in WSMs [13,14,20–23], where E_F is the Fermi energy. The observation of the chiral anomaly in solid states not only is of great conceptual interest but also paves the way for realizing high-speed electronic circuits and computers [66–68]. Therefore, in recent years, great efforts have been devoted to searching for evidence of the chiral anomaly in various Weyl materials [69–71].

The semiclassical Boltzmann approach has been widely adopted to study chiral-anomaly-related transport in WSMs, but it predicts an unphysical diverging positive LMC when $E_F \to 0$. In addition, the Boltzmann approach focuses mainly on nonequilibrium electron transport after the steady state has been established, while the circumstances before the steady

*dengmingxun@scnu.edu.cn
†wangruiqiang@m.scnu.edu.cn

state is formed have been considered less. In the ultraquantum limit, it is known that the chiral anomaly is attributed to the zeroth chiral Landau levels (LLs) and the resulting positive LMC exhibits an E_F-independent plateau for $|E_F| < \sqrt{2}\hbar\omega_c$, with ω_c being the cyclotron frequency [19,71]. Besides the conflict between the classical and ultraquantum limits, a unified classical theory across these two limits to understand the chiral anomaly is still lacking. Additionally, another natural question is whether the $\boldsymbol{E} \cdot \boldsymbol{B}$ term is essential for the chiral anomaly. Recently, Rylands *et al.* showed that the electric and magnetic fields on the right-hand side of Eq. (1) can be modified by the fluctuations induced by interacting matter [64]. Although the right hand side of Eq. (1) still emerges in the form $\tilde{E} \cdot \tilde{B}$, with $\tilde{E}$ and $\tilde{B}$ being, respectively, the effective electric and magnetic fields in the presence of interactions, their result implies an alternative path to determine the chiral anomaly.

In this paper, we draw a connection between the chiral anomaly and the topological pumping effect [72–75] by deriving a modified semiclassical EOM including the off-diagonal contribution of the Berry curvature. Based on this, we study magnetotransport in WSMs beyond the Boltzmann approach. We find that a magnetic field couples with the Berry curvature by driving the fermions to rotate around the Weyl nodes, during which time the Weyl fermions will acquire a Berry phase to induce the CME. Upon application of parallel electric and magnetic fields, the chemical potential will increase in one valley but decrease in the other. As a result, a chiral chemical potential will be established between the Weyl valleys, which in turn breaks the chiral symmetry and generates the positive LMC. With the topological pumping mechanism, we further demonstrate that the chiral anomaly can be realized even without $\boldsymbol{E} \cdot \boldsymbol{B}$. More importantly, our theory successfully overcomes the difficulty of the unphysical divergence predicted by the Boltzmann theory, bridging the gap between the classical and ultraquantum approaches. The rest of this paper is organized as follows. In Sec. II, we introduce the model and method. The magnetic-field-driving CME and chiral anomaly are discussed, respectively, in Secs. III and IV. The ac electric-field-driving chiral anomaly is discussed in Sec. V, and the last section contains a short summary.

II. MODEL AND METHOD

We start with a general low-energy description,

$$\mathcal{H}_{\mathrm{w}}(\boldsymbol{k}) = \chi\hbar\upsilon_F \boldsymbol{\sigma} \cdot \boldsymbol{k}, \qquad (2)$$

for the WSMs, where $\chi = \pm$ represent two Weyl nodes of opposite chiralities, $\boldsymbol{\sigma} = (\sigma_x, \sigma_y, \sigma_z)$ denotes the vector of the Pauli matrix, and $\boldsymbol{k}$ is the wave vector measured from the Weyl nodes. Diagonalizing Eq. (2) yields the energy spectrum $\varepsilon_{\boldsymbol{k},s}^{\chi} = s\hbar\upsilon_F k$, where $s = \pm$ label the conduction and valence bands and $k = \sqrt{k_x^2 + k_y^2 + k_z^2}$ accounts for the magnitude of the wave vector. The corresponding wave function is $\psi_s^{\chi}(\boldsymbol{k}) = (\cos\varphi, \sin\varphi e^{i\phi})^T$, where $\varphi = \frac{\theta}{2} + \frac{1-s\chi}{4}\pi$, with $\theta = \cos^{-1}(k_z/k)$ and $\phi = \tan^{-1}(k_y/k_x)$. As the Weyl fermions are coupled to external fields, the system can be captured by

$$H = \mathcal{H}_{\mathrm{w}}(\boldsymbol{k}) - \boldsymbol{j}(\boldsymbol{r}) \cdot \boldsymbol{A} - e\Phi, \qquad (3)$$

in which $\boldsymbol{A}$ (Φ) denotes the electromagnetic vector (scalar) potential and $\boldsymbol{j}(\boldsymbol{r}) = -e\dot{\boldsymbol{r}}$ is the charge current density operator. The external fields are assumed to be homogeneous in real space.

For convenience, we rewrite the Hamiltonian as an explicit function of the external fields as $H = \mathcal{H}_{\mathrm{w}}(\boldsymbol{k}) - \boldsymbol{F} \cdot \boldsymbol{r}$, where the generalized force is defined as [76]

$$\boldsymbol{F} = -\nabla U(\boldsymbol{r}, \dot{\boldsymbol{r}}) + \frac{d}{dt}\frac{\partial U(\boldsymbol{r}, \dot{\boldsymbol{r}})}{\partial \dot{\boldsymbol{r}}}, \qquad (4)$$

with $U(\boldsymbol{r}, \dot{\boldsymbol{r}}) = e\dot{\boldsymbol{r}} \cdot \boldsymbol{A} - e\Phi$. Using the Heisenberg EOM $i\hbar\dot{O} = [O, \mathcal{H}(\boldsymbol{k})]$, we can derive for $\dot{\boldsymbol{r}} = \hbar^{-1}\nabla_{\boldsymbol{k}}\mathcal{H}_{\mathrm{w}}(\boldsymbol{k})$ and $\dot{\boldsymbol{k}} = \hbar^{-1}\boldsymbol{F}$. Then, the expectation of $\dot{\boldsymbol{r}}$ can be evaluated by

$$\langle\psi_s^{\chi}(t)|\dot{\boldsymbol{r}}|\psi_s^{\chi}(t)\rangle = \sum_p \langle\psi_p^{\chi}|\dot{\boldsymbol{r}}\rho(t)|\psi_p^{\chi}\rangle, \qquad (5)$$

where $\rho(t) = |\psi_s^{\chi}(t)\rangle\langle\psi_s^{\chi}(t)|$ is the density matrix operator and ψ_s^{χ} $[\psi_s^{\chi}(t)]$ denotes the wave function in the absence (presence) of the external perturbation $U(\boldsymbol{r}, \dot{\boldsymbol{r}}) = -\hbar\dot{\boldsymbol{k}} \cdot \boldsymbol{r}$.

Within linear-response theory, we can express the perturbed density matrix as $\rho(t) = \rho_0 + \rho_1(t)$, where $\rho_0 = |\psi_s^{\chi}\rangle\langle\psi_s^{\chi}|$ is the equilibrium density matrix and

$$\rho_1(t) = -\frac{i}{\hbar}\int_{-\infty}^t dt' [e^{-i\mathcal{H}_{\mathrm{w}}(t-t')/\hbar}U(\boldsymbol{r}, \dot{\boldsymbol{r}})e^{i\mathcal{H}_{\mathrm{w}}(t-t')/\hbar}$$
$$\times \rho_0 - \rho_0 e^{-i\mathcal{H}_{\mathrm{w}}(t-t')/\hbar}U^{\dagger}(\boldsymbol{r}, \dot{\boldsymbol{r}})e^{i\mathcal{H}_{\mathrm{w}}(t-t')/\hbar}]. \qquad (6)$$

Subsequently, we can obtain (see Appendix A)

$$\hat{\dot{\boldsymbol{k}}} = -\frac{e}{\hbar}\boldsymbol{E} - \frac{e}{\hbar}\hat{\dot{\boldsymbol{r}}} \times (\nabla \times \boldsymbol{A}), \qquad (7a)$$

$$\hat{\boldsymbol{r}} = \langle\Psi|\frac{\partial\mathcal{H}_{\mathrm{w}}(\boldsymbol{k})}{\hbar\partial\boldsymbol{k}}|\Psi\rangle - \bigoplus_s \mathrm{Tr}[\hat{\dot{\boldsymbol{k}}} \times \hat{\boldsymbol{\Omega}}_s(\boldsymbol{k})], \qquad (7b)$$

with $\boldsymbol{E} = -\nabla\Phi - \partial_t\boldsymbol{A}$, where the operators are 2×2 matrices in the Hilbert space $\Psi = \{|\psi_+^{\chi}\rangle, |\psi_-^{\chi}\rangle\}$, e.g., $\hat{O} = \langle\Psi|O|\Psi\rangle$, with $O = \{\boldsymbol{r}, \dot{\boldsymbol{r}}, \dot{\boldsymbol{k}}\}$, and $\hat{\boldsymbol{\Omega}}_s(\boldsymbol{k}) = -i\langle\Psi|\boldsymbol{r}|\psi_s^{\chi}\rangle \times \langle\psi_s^{\chi}|\boldsymbol{r}|\Psi\rangle$. Different from the conventional semiclassical EOM, Eq. (7) includes the off-diagonal contribution of the Berry curvature. Without the off-diagonal elements of $\hat{\boldsymbol{\Omega}}_s(\boldsymbol{k})$, the last term in Eq. (9) reduces to $\hat{\dot{\boldsymbol{k}}} \times i(\hat{\boldsymbol{r}} \times \hat{\boldsymbol{r}})$. In classical mechanics, this term vanishes for the vector algorithm in plane geometry, and $\hat{\boldsymbol{r}} = \langle\Psi|\partial_{\boldsymbol{k}}\mathcal{H}_{\mathrm{w}}/\hbar|\Psi\rangle$ returns to the classical limit. However, in quantum mechanics, the vector is defined in the Hilbert space, in which $\boldsymbol{r}$ is an operator acting on the basic wave functions, such that $\hat{\boldsymbol{r}} \times \hat{\boldsymbol{r}}$ can be nonvanishing, especially for topological electronic structures. For example, in momentum space, $\hat{\boldsymbol{r}} \rightarrow i\langle\Psi|\nabla_{\boldsymbol{k}}|\Psi\rangle$ becomes the Berry connection, and $\hat{\boldsymbol{\Omega}}_{\boldsymbol{k}} \equiv -i(\hat{\boldsymbol{r}} \times \hat{\boldsymbol{r}}) = (\eta_x \cot\theta - \eta_z)\chi\boldsymbol{k}/(2k^3)$ defines the Berry curvature, where $\eta_{x,y,z}$ represents the Pauli matrix for the Ψ Hilbert space. Then, with the relation $\boldsymbol{B} = \nabla \times \boldsymbol{A}$, the diagonal part of Eq. (7) recovers the well-known quasiclassical EOM derived from the wave packet dynamics [65].

In the adiabatic approximation, the external fields regulate Ψ slowly by the replacement $\boldsymbol{k} \rightarrow \boldsymbol{k}(t)$. In this situation, we can approximate $\dot{\boldsymbol{k}} \cdot \boldsymbol{r} \rightarrow i\partial_t$, which means neglecting the off-diagonal elements of $\dot{\boldsymbol{k}}$, such that Eq. (7b) recovers the velocity $\hat{\upsilon}_{\alpha}^{\chi}(\boldsymbol{k}, t) = \partial\mathcal{H}_{\boldsymbol{k}}/\hbar\partial k_{\alpha} - \hat{\Pi}_{\alpha}(\boldsymbol{k}, t)$ for the adiabatic

pumping current density [65]

$$j_{P,\alpha}^{\chi} = -\frac{e}{V} \sum_{\boldsymbol{k}} \frac{1}{\mathcal{T}} \int_0^{\mathcal{T}} dt \, \mathrm{Tr}\big[\hat{v}_\alpha^\chi(\boldsymbol{k},t) f(\mathcal{H}_{\boldsymbol{k}})\big], \qquad (8)$$

where $\mathcal{H}_{\boldsymbol{k}} = \mathrm{diag}(\varepsilon_{\boldsymbol{k},+}^\chi, \varepsilon_{\boldsymbol{k},-}^\chi)$ and $\hat{\Pi}_\alpha(\boldsymbol{k},t) = i[\langle \partial_{k_\alpha}\Psi | \partial_t \Psi \rangle - \langle \partial_t \Psi | \partial_{k_\alpha}\Psi \rangle]$ is the Berry curvature defined in the k_α-t parameter space, with $V = L_x L_y L_z$ being the sample's volume, $f(\epsilon) = [1 + e^{\beta(\epsilon - E_F)}]^{-1}$ being the electron distribution function, and $\beta^{-1} = k_B T$ being the thermal fluctuation energy. The velocity of the carriers, owing to

$$\hat{\Pi}_\alpha(\boldsymbol{k},t) = -\chi\eta_\theta \frac{\eta_z \epsilon_{\alpha\beta\gamma} \dot{k}_\beta(t) k_\gamma(t)}{2\big[k_x^2(t) + k_y^2(t) + k_z^2(t)\big]^{\frac{3}{2}}}, \qquad (9)$$

can be chirality dependent, where $\eta_\theta = \eta_0 + i\eta_y \cot\theta$ and $\epsilon_{\alpha\beta\gamma}$ is the Levi-Civita antisymmetric tensor.

III. MAGNETIC-FIELD-DRIVING CME

For simplicity, we fix $\boldsymbol{B} = B\hat{e}_z$ and turn off the electric field by setting $\boldsymbol{E} = 0$. In the adiabatic approximation, we can derive for

$$\frac{\partial k_\alpha}{\partial t} = -s \frac{eB\upsilon_F}{\hbar k} \epsilon_{\alpha\beta z} k_\beta + \mathcal{O}(B^2). \qquad (10)$$

The magnetic field itself does not alter the electrons' energy, so k remains unchanged. By differentiating both sides of Eq. (10) with respect to t, we can obtain the equation of simple harmonic motion $\partial_t^2 k_{x,y} + \omega_k^2 k_{x,y} = 0$, with $\omega_k = eB\upsilon_F/(\hbar k)$ being the angular frequency. Subsequently, we can solve for $k_{x,y}(t) = k_{x,y}|_{\phi \to \phi + s\omega_k t}$, such that the coordinate-dependent vector potential $\boldsymbol{A}$ can be equivalent to a time-dependent vector potential with $e\hbar^{-1}\partial_t A_{x,y} = \partial_t k_{x,y}$. In other words, the magnetic field acts like an in-plane rotating electric field driving the wave vector to circle around the Weyl nodes. While a Bloch electron rotates around the monopole in momentum space, it would acquire a Berry phase, causing the topological pumping effect. Therefore, we would expect current to be pumped by the magnetic field itself, manifesting the CME.

Importantly, the rotating direction of the wave vectors in the valence band is opposite to that in the conduction band. Meanwhile, the Berry curvatures in the conduction and valence bands also have opposite signs. Hence, the pumping direction, as demonstrated below, will be identical for the conduction and valence bands. By substituting $k_{x,y}(t)$ into Eq. (9), we find

$$\hat{v}_\alpha^\chi(\boldsymbol{k},t) = \eta_z \upsilon_F \frac{k_\alpha}{k} - \chi\eta_\theta \frac{eB\upsilon_F}{2\hbar k^2}\left(\delta_{\alpha,z} - \frac{k_z k_\alpha}{k^2}\right), \qquad (11)$$

with $\ell_B = \sqrt{\hbar/eB}$ being the magnetic length. We see that, although the driven wave vector $k_{x,y}(t)$ is time dependent, the anomalous velocity $\hat{\Pi}_z(\boldsymbol{k},t) = \chi\eta_\theta \upsilon_F \sin^2\theta / (2\ell_B^2 k^2)$ is time independent, which indicates a uniform-speed pumping process. It is in contrast to the variable-speed pumping for the ac electric field because the Hilbert space here driven by the magnetic field rotates with a constant speed, during which time the electrons feel identical strength of the Berry curvature, as shown by Figs. 1(a) and 1(b), where the fermions move along the latitude of the energy contour. The Weyl nodes, as the center of the energy contour, are always within the
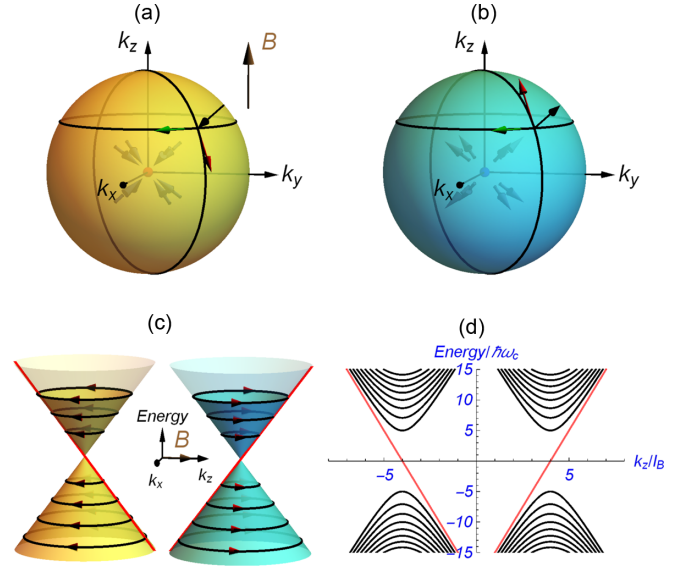
FIG. 1. (a) and (b) Schematics for the pumping process of the Weyl fermions with magnetic field. The yellow (cyan) sphere represents the Fermi surface of the Weyl valley with positive (negative) chirality, on which the black, green, and red arrows indicate, respectively, the direction of the Berry curvature, magnetic-induced effective electric field, and anomalous velocity. (c) The Weyl cones for $k_y = 0$, with the black circles denoting the energy contour and the arrows indicating the direction of the anomalous velocity, where the red lines correspond to the chiral LLs in (d).

closed path of the electrons. Consequently, for magnetic field driving, all the states below the Fermi surface will contribute to the pumping, as demonstrated by Fig. 1(c). However, for ac electric field driving, as discussed in Sec. V, the Weyl cones are shifted integrally along the electric field, and equivalently, the driven electrons will rotate around an in-plane wave vector, as illustrated by Fig. 2(c). During this process, the Weyl fermions change their energy and feel different strengths of the Berry curvature, thus causing a variable-speed pumping process. Moreover, when $k_x^2 + k_y^2 > k_c^2$, with $k_c = eE_\perp/(\hbar\omega)$ determined by the ac electric field [for example, the green lines in Fig. 2(c)], the Weyl nodes are out of the electrons' closed path and therefore make no contribution to the pumping effect. This also can be seen from the numerical results presented in Fig. 2(d). In this sense, the pumping efficiency of the magnetic field is much higher than that of the ac electric field.

Actually, the physical picture from Eq. (7) can be more intuitive. For example, if only the diagonal contribution is included, the solution to Eq. (7) is $\hat{k} = -e\boldsymbol{E}_{\mathrm{eff}}/\hbar$, and

$$\hat{r} = \frac{\partial \mathcal{H}_{\boldsymbol{k}}}{\hbar \partial \boldsymbol{k}} + \frac{e}{\hbar} \boldsymbol{E}_{\mathrm{eff}} \times \hat{\boldsymbol{\Omega}}_{\boldsymbol{k}}, \qquad (12)$$

where the effective electric field is $\boldsymbol{E}_{\mathrm{eff}} = D_{\boldsymbol{k}} \hbar^{-1} \partial_{\boldsymbol{k}} \mathcal{H}_{\boldsymbol{k}} \times \boldsymbol{B}$, with $D_{\boldsymbol{k}} = (1 + e\boldsymbol{B} \cdot \hat{\boldsymbol{\Omega}}_{\boldsymbol{k}}/\hbar)^{-1}$. The Berry curvature and effective electric field are schematically shown in Figs. 1(a) and 1(b). As illustrated by Figs. 1(a) and 1(b), when the magnetic field drives the Bloch electrons moving along the latitude of the energy contour, the Berry curvature will induce a tangent anomalous velocity along the longitude, as illustrated by the
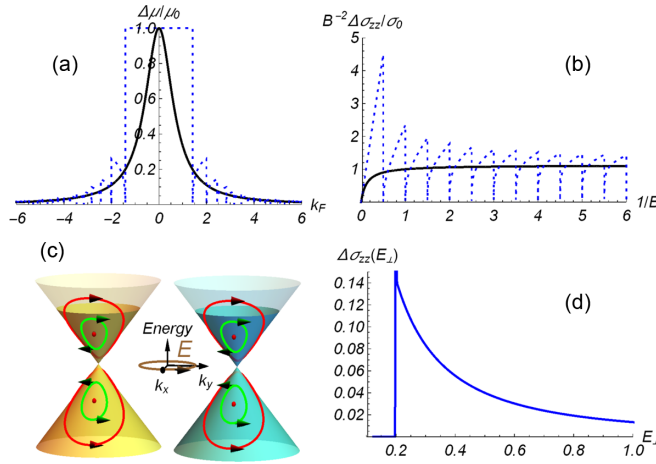
FIG. 2. (a) The chiral chemical potential vs k_F and (b) the LMC vs $1/B$, with $\mu_0 = eE_z \upsilon_F \tau$ and $\sigma_0 = \Delta\sigma_{zz}(B = 1\text{T})$. The black solid and blue dashed lines represent the results obtained from the classical and ultraquantum limits, respectively. (c) Schematic of the ac electric field pumping process, in which the left (right) cone is plotted for the positive (negative) Weyl valley, and (d) $\Delta\sigma_{zz}(E_\perp)$ as a function of $E_\perp$, with the jumping point corresponding to $k_c = k_F$.

red arrows in Figs. 1(a) and 1(b). To leading order in magnetic field, the velocity given by Eq. (12) equals Eq. (11). Above, because the off-diagonal contribution of the Berry curvature has been neglected, the pumping current density for a given energy is quantized to $2\chi/3$ in units of Be^2/h^2 [see Eq. (A14)]. If the off-diagonal elements in Eq. (7) are included, the z component of the velocity becomes

$$\hat{\upsilon}_z^\chi(\mathbf{k}, t) = \eta_z \upsilon_F \frac{k_\alpha}{k} - \chi \frac{eB\upsilon_F}{2\hbar k^2}(1 + \chi\eta_z \cos\theta). \tag{13}$$

Then, the pumping current density on the Fermi surface is quantized exactly to the topological charge χ, as demonstrated by Eq. (A16), which characterizes the topological property of the WSMs more robustly.

As discussed above, each constant-energy surface enclosing the Weyl node will contribute a quantized current density $\chi Be^2/h^2$. Therefore, at low temperatures with $f(\varepsilon_{\mathbf{k},s}^\chi) \simeq \Theta(E_F - \varepsilon_{\mathbf{k},s}^\chi)$, by summing over all the contributions below the Fermi level, we can estimate the chirality-resolved current density as

$$j_{P,\alpha}^\chi = \chi \frac{e^2}{h} \frac{E_\Lambda + E_F}{h} B\delta_{\alpha,z}, \tag{14}$$

where E_Λ is an energy cutoff for the linear dispersion. Equation (14) shows that the magnetic field can indeed pump current $\propto \mathbf{B}$ as a characteristic phenomenon of the CME. The pumping current satisfies the symmetry $j_{P,z}^\chi = -j_{P,z}^{-\chi}$; namely, it flows in opposite directions for Weyl valleys of opposite chirality, so the net charge current will vanish. As the chiral symmetry is broken, e.g., the Weyl nodes are separated in energy by b_0 or a chiral chemical potential $\Delta\mu$ is established between the Weyl valleys, nonvanishing charge current $j_{P,z}^c = b_0 Be^2/h^2$ or $2\Delta\mu Be^2/h^2$ can be measured. This is consistent with the prediction of topological field theory.

IV. MAGNETIC-FIELD-DRIVING CHIRAL ANOMALY

Intuitively, charge current will emerge if an additional electric field is applied along the pumping direction because when the Bloch electrons in opposite Weyl valleys are pumped along or against the electric field, the chemical potential will decrease in one valley but increase in the other. Then, the chiral symmetry will be broken, and a chiral chemical potential could be established between the Weyl valleys and further lead to observable charge current. To verify this argument, we apply an electric field $E_z = -\partial_t A_z$ along the z direction. The Hamiltonian according to Eq. (3) becomes

$$\tilde{H}_{\mathbf{k}} = \mathcal{H}_{\mathbf{k}} + \int_0^t dt' j_z(\mathbf{r}) E_z e^{-\Gamma t'/\hbar}, \tag{15}$$

with $\tau = \hbar/\Gamma$ being the lifetime of the fermions and $j_z(\mathbf{r}) = -e\hat{\upsilon}_z^\chi(\mathbf{k}, t)$ given by Eq. (13). Since the Berry curvature is ill defined for $k = 0$, $\varepsilon_{\mathbf{k},s}^\chi = 0$ is a singularity of the distribution function $f(\tilde{\varepsilon}_{\mathbf{k},s}^\chi)$, with $\tilde{\varepsilon}_{\mathbf{k},s}^\chi$ being the energy for $\tilde{H}_{\mathbf{k}}$. Therefore, the Taylor expansion $f(\tilde{\varepsilon}_{\mathbf{k},s}^\chi) \simeq f(\varepsilon_{\mathbf{k},s}^\chi) + g_{\mathbf{k}}^\chi \frac{\partial f(\varepsilon_{\mathbf{k},s}^\chi)}{\partial \varepsilon_{\mathbf{k},s}^\chi}$ breaks down at $\varepsilon_{\mathbf{k},s}^\chi = 0$, leading to invalidation of the Boltzmann approach. This is the origin of the unphysical diverging electrical conductivity in the Boltzmann theory. This issue can be addressed as follows.

Due to the topological electronic structure, a weak magnetic field will separate the spectrum into two parts: a part with achiral dispersion $\varepsilon_{\mathbf{k},s}^\chi \simeq s\hbar\upsilon_F k$ which maintains the shape of the Weyl cone and possesses chirality-dependent Berry curvature and another part with chiral dispersion $\varepsilon_{k_z,0}^\chi = -\chi\hbar\upsilon_F k_z$ but without Berry curvature. Details are presented in Appendix B. Consequently, the achiral dispersion, i.e., the Weyl cone, acquires an anomalous velocity at each $\mathbf{k}$ point, as if it were decorated with chiral channels, as shown by Figs. 1(a)–1(c). Upon application of parallel electric and magnetic fields, the chemical potential, by averaging the second term in Eq. (15) over the Fermi surface, will change by

$$\Delta\mu_\chi = \frac{\hbar}{\tilde{\Gamma}} \frac{-eE_z \sum_{\mathbf{k}s} \hat{\upsilon}_{s,z}^\chi(\mathbf{k}, t)\delta(E_F - \varepsilon_{\mathbf{k},s}^\chi)}{\sum_{\mathbf{k}s} \delta(E_F - \varepsilon_{\mathbf{k},s}^\chi) + \sum_{k_z} \delta(E_F - \varepsilon_{k_z,0}^\chi)}, \tag{16}$$

with $\tilde{\Gamma} = \Gamma/(1 - e^{-\Gamma t/\hbar})$, so that the Fermi energy will be renormalized. It can be verified that the density of states (DOS) of the chiral channels satisfies the identity

$$N_{\text{ch}} \equiv \sum_{k_z} \delta(E_F - \varepsilon_{k_z,0}^\chi) = \left| \sum_{\mathbf{k}s} \frac{\hat{\upsilon}_{s,z}^\chi(\mathbf{k}, t)}{\upsilon_F} \delta(E_F - \varepsilon_{\mathbf{k},s}^\chi) \right|. \tag{17}$$

Accordingly, we can express the chiral chemical potential as

$$\Delta\mu = \frac{\hbar}{\tilde{\Gamma}} \frac{eE_z \upsilon_F}{1 + N_{\text{ch}}^{-1} \sum_{\mathbf{k}s} \delta(E_F - \varepsilon_{\mathbf{k},s}^\chi)}. \tag{18}$$

In the diffusive regime, the system reaches the steady state rapidly by impurity scattering, such that we can replace $t \to \infty$ and obtain for the steady state Fermi energy $E_F + \chi\Delta\mu$ with the chiral chemical potential

$$\Delta\mu = \frac{eE_z \upsilon_F \tau}{1 + 2\ell_B^2 k_F^2}. \tag{19}$$

Consequently, the steady-state LMC reads

$$\Delta\sigma_{zz}(B) \equiv \frac{j_{P,z}^{+} + j_{P,z}^{-}}{E_z} = \frac{2e^2}{h}\frac{1}{2\pi\ell_B^2}\frac{\upsilon_F\tau}{1+2\ell_B^2 k_F^2}. \qquad (20)$$

Obviously, the LMC is no longer divergent when $E_F \rightarrow 0$, which also can be seen from Fig. 2(a). In the ballistic regime where the travel time of the Weyl fermions is far smaller than the relaxation time, i.e., $d < \hbar\upsilon_F/\Gamma$, with d being the distance between the measuring electrodes, the LMC $\propto d$, while its magnetic field and E_F dependences remain unchanged.

For $2\ell_B^2 k_F^2 \gg 1$, Eq. (20) can be approximated as

$$\Delta\sigma_{zz}(B) = \frac{e^2}{4\pi^2\hbar}\frac{(eB)^2\upsilon_F^2}{E_F^2}\upsilon_F\tau, \qquad (21)$$

which exhibits a B^2-dependent positive LMC scaled with $1/E_F^2$. This is exactly the expression derived by the semiclassical Boltzmann approach [13,14,20–23]. In the opposite limit, i.e., $2\ell_B^2 k_F^2 \ll 1$, we can reduce Eq. (20) to

$$\Delta\sigma_{zz}(B) = \frac{e^2}{2\pi^2\hbar}\frac{eB\upsilon_F\tau}{\hbar}, \qquad (22)$$

which predicts a B-dependent and E_F-scaled unsaturated LMC. This expression recovers the one derived in the ultraquantum limit [19,71]. In the ultraquantum limit, the spectra are quantized to the LLs, and by replacing $k_F^2 \rightarrow \ell_B^{-2}\sum_{n=1}^{[\ell_B^2 k_F^2/2]}[1 - 2n/(\ell_B^2 k_F^2)]^{-\frac{1}{2}}$, the positive LMC will exhibit the periodic-in-$(1/B)$ quantum oscillations, as shown by Figs. 2(a) and 2(b). Therefore, within our theory, the results in the semiclassical and ultraquantum limits are consistent with each other.

V. ac ELECTRIC-FIELD-DRIVING CHIRAL ANOMALY

From the discussions above, we know that the chiral anomaly, in fact, has a topological pumping origin because the Bloch electrons are driven by the magnetic field to rotate around the Weyl nodes. With this mechanism, we can realize the chiral anomaly using a compound electric field instead of a magnetic field.

To demonstrate this point, we turn off the magnetic field in the following and assume a rotating electric field is applied to the x-y plane, i.e., $E_x(t) = E_\perp \sin\omega t$ and $E_y(t) = -E_\perp \cos\omega t$. In the adiabatic approximation, the wave vector according to Eq. (7a) will be renormalized as $k_x(t) = k_x + k_c\cos\omega t$ and $k_y(t) = k_y + k_c\sin\omega t$, where $k_c = eE_\perp/(\hbar\omega)$. The time-dependent spectrum is given by

$$\tilde{\varepsilon}_{\boldsymbol{k},s}^{\chi} = s\hbar\upsilon_F\sqrt{k_x^2(t) + k_y^2(t) + k_z^2}. \qquad (23)$$

The gap-closing point according to Eq. (23) is modified to $\boldsymbol{k}_w = -k_c(\cos\omega t, \sin\omega t, 0)$, so that the Weyl cones are shifted integrally along the electric field. Equivalently, the driven electrons for a given wave vector will rotate around an in-plane wave vector, as shown by the red and green lines in Fig. 2(c). During this process, the Weyl fermions change their energy and feel different strengths of the Berry curvature. As a result, the anomalous velocity

$$\Pi_z^{s,\chi}(\boldsymbol{k},t) = s\chi\frac{eE_\perp}{\hbar}\frac{k_y(t)\sin\omega t + k_x(t)\cos\omega t}{2[k_x^2(t) + k_y^2(t) + k_z^2]^{\frac{3}{2}}} \qquad (24)$$

is time dependent, which implies a variable-speed pumping process. Over a pumping period $\mathcal{T} = 2\pi/\omega$, the averaged current density is given by

$$j_{P,z}^{\chi} = \frac{e\omega}{2\pi V}\int_0^{\mathcal{T}} dt \sum_{\boldsymbol{k}s}\Pi_z^{s,\chi}(\boldsymbol{k},t)f(\tilde{\varepsilon}_{\boldsymbol{k},s}^{\chi}). \qquad (25)$$

For the purpose of illustration, we first consider the case of ideal WSMs, whose Fermi level locates exactly at the Weyl nodes. At low temperatures, we can reduce Eq. (25) to

$$j_{P,z}^{\chi} = \frac{e\omega}{2\pi}\frac{1}{4\pi^2}\int_{-\infty}^{\infty} dk_x \int_{-\infty}^{\infty} dk_y C_\chi(k_x, k_y), \qquad (26)$$

where the Chern number

$$C_\chi(k_x, k_y) = \frac{1}{2\pi}\int_0^{\mathcal{T}} dt \int_{-\infty}^{\infty} dk_z \Pi_z^{-,\chi}(\boldsymbol{k},t) \qquad (27)$$

is constructed by the torus of the two variables $k_z \in (-\infty, \infty)$ and $t \in [0, \mathcal{T}]$. Subsequently, we can derive for

$$C_\chi(k_x, k_y) = \chi\Theta(k_c^2 - k_x^2 - k_y^2). \qquad (28)$$

Hence, the pumping current density in the χ valley reads

$$j_{P,z}^{\chi} = \chi\frac{e^2}{4\pi h}\frac{eE_\perp^2}{\hbar\omega}. \qquad (29)$$

From Eq. (29), we see that an out-of-plane current can be pumped by the in-plane rotating electric field. However, similar to the case of magnetic field driving, the net pumping current vanishes for the chiral symmetry $j_{P,z}^{\chi} = -j_{P,z}^{-\chi}$. Actually, even for finite $E_F \neq 0$, the charge current can be expected to be vanishing because of the symmetries $\Pi_z^{s,\chi}(\boldsymbol{k},t) = -\Pi_z^{s,-\chi}(\boldsymbol{k},t)$ in Eq. (25).

Analogously, if we apply an additional electric field E_z along the z direction, the Fermi energy, resembling Eq. (16), will change by

$$\Delta\mu_\chi = \frac{-eE_z\tau\sum_{\boldsymbol{k}s}\Pi_z^{s,\chi}(\boldsymbol{k},t)\delta(E_F - \varepsilon_{\boldsymbol{k},s}^{\chi})}{N_{\text{ch}}' + \sum_{\boldsymbol{k}s}\delta(E_F - \varepsilon_{\boldsymbol{k},s}^{\chi})}. \qquad (30)$$

Here, the DOS of the chiral channels is given by $N_{\text{ch}}' = |\sum_{\boldsymbol{k}s}\Pi_z^{s,\chi}(\boldsymbol{k},t)\delta(E_F - \varepsilon_{\boldsymbol{k},s}^{\chi})/\upsilon_F|$. Accordingly, the chiral chemical potential, as defined by Eq. (18), is given by

$$\Delta\mu = \frac{eE_z\tau}{1 + \sum_{\boldsymbol{k}s}\delta(E_F - \varepsilon_{\boldsymbol{k},s}^{\chi})/N_{\text{ch}}'} = \frac{eE_z\upsilon_F\tau}{1 + 2\ell_\perp^2 k_F^2}, \qquad (31)$$

where $\ell_\perp = \sqrt{\hbar\upsilon_F/(eE_\perp|\mathcal{F}|)}$ and

$$\mathcal{F} = \frac{1}{4\pi}\int_0^{\pi} d\theta \int_0^{2\pi} d\phi\frac{\lambda\sin\theta + \sin^2\theta\cos\phi_t}{[1 + \lambda^2 + 2\lambda\sin\theta\cos\phi_t]^{\frac{3}{2}}}, \qquad (32)$$

with $\phi_t = \phi - \omega t$ and $\lambda = k_c/k_F$. After the angular integral, $\mathcal{F}$ is time independent. Then, the pumping charge current density takes the form

$$j_{P,z}^c = \frac{e}{V}\sum_{\boldsymbol{k}s\chi}\Pi_z^{s,\chi}(\boldsymbol{k},t)f(\varepsilon_{\boldsymbol{k},s}^{\chi} - \chi\Delta\mu)$$

$$= \frac{2e}{h}\frac{1}{2\pi\ell_\perp^2}\frac{eE_z\upsilon_F\tau}{1 + 2\ell_\perp^2 k_F^2}. \qquad (33)$$

As can be seen, the out-of-plane component E_z breaks the chiral symmetry and then generates an observable charge current.

Or we can say that, with the in-plane ac electric field turned on, the out-of-plane conductivity will increase by

$$
\begin{aligned}
\Delta\sigma_{zz}(E_\perp) &\equiv \left[j^c_{P,z}(E_\perp) - j^c_{P,z}(E_\perp = 0) \right]/E_z \\
&= \frac{2e}{h} \frac{1}{2\pi \ell_\perp^2} \frac{e v_F \tau}{1 + 2\ell_\perp^2 k_F^2}.
\end{aligned}
\tag{34}
$$

As plotted in Fig. 2(d), $\Delta\sigma_{zz}(E_\perp)$ exhibits a step change at $k_c = k_F$ because the trajectory of the Bloch electrons on the Fermi surface cannot encircle the Weyl nodes for $k_c < k_F$ [see Fig. 2(c)]. For $k_c > k_F$, the electron states on the Fermi surface will be activated to contribute the topological pumping effect. Therefore, the step change of $\Delta\sigma_{zz}(E_\perp)$ with respect to k_c can serve as a signal of the chiral anomaly. Different from the magnetic-field-driving case, the wave vectors driven by the ac electric field rotate in the same direction for the conduction and valence bands. Therefore, the contributions from the conduction and valence bands possess opposite signs and will cancel each other. For a finite Fermi energy crossing the conduction band, as we increase k_c, the contribution from the conduction band will be canceled more and more by the valence band, and as a result, $\Delta\sigma_{zz}(E_\perp)$ decreases with increasing k_c.

To observe the proposed phenomenon, the angular frequency of the ac electric field should fulfill the condition $\omega \geqslant 2\pi/\tau$, which ensures that the electrons have accomplished a complete cyclotron motion with respect to the Weyl node before being scattered by impurities. At low temperature, the measured relaxation time in WSMs is $\tau \sim 45$ps [77,78], corresponding to the frequency ($\sim 2\times 10^{10}$ Hz) of a microwave. Therefore, microwave or far-infrared light could be the appropriate frequency for experimental observation. The circular photogalvanic effect in WSMs has been studied previously, such as in Refs. [78,79]. In these theories, the photovoltaic effects were realized either by transfer of the photon angular momentum to electrons or finite tilts of the Weyl cone, which require intrinsic broken chiral or inversion symmetry

in the spectrum. In contrast, the mechanism studied here does not involve the above intrinsic symmetry-breaking or photon absorption/emission process. The chiral chemical potential here is established by the joint effect of the external electric field and adiabatic dynamics of electron orbitals. The light-induced conductivity increment is attributed to the pumping effect because of the Berry phase that arises from the non-trivial change in the Bloch wave function over a period of the pumping cycle.

VI. CONCLUSION

In summary, we developed a modified semiclassical EOM with the off-diagonal contribution of the Berry curvature included, with which we derived a unified formula across the classical and ultraquantum regimes for the chiral chemical potential and LMC. Our formula avoids the unphysical divergence in the Boltzmann theory and bridges the gap between the classical and ultraquantum approaches. We demonstrated that the chiral anomaly in WSMs is closely related to the topological pumping effect, and with the topological pumping mechanism, we showed that the chiral anomaly can be realized in the absence of magnetic field.

APPENDIX A: DERIVATION OF THE SEMICLASSICAL EQUATION OF MOTION

By substituting Eq. (6) into Eq. (5), we can derive

$$
\begin{aligned}
\langle\psi_s^\chi(t)|\dot{r}|\psi_s^\chi(t)\rangle &= \langle\psi_s^\chi|\dot{r}|\psi_s^\chi\rangle - \frac{i}{\hbar}\int_0^\infty d\tau \langle\psi_s^\chi|\left[\dot{r}e^{-i\mathcal{H}_w\tau/\hbar}U(r)e^{i\mathcal{H}_w\tau/\hbar} - e^{-i\mathcal{H}_w\tau/\hbar}U^\dagger(r)e^{i\mathcal{H}_w\tau/\hbar}\dot{r}\right]|\psi_s^\chi\rangle \\
&= \langle\psi_s^\chi|\frac{\partial\mathcal{H}_w(\mathbf{k})}{\hbar\partial\mathbf{k}}|\psi_s^\chi\rangle + \sum_p \left[\langle\psi_s^\chi|\partial_{\mathbf{k}}|\psi_p^\chi\rangle\langle\psi_p^\chi|\dot{\mathbf{k}}\cdot\mathbf{r}|\psi_s^\chi\rangle - \langle\psi_s^\chi|\mathbf{r}\cdot\dot{\mathbf{k}}|\psi_p^\chi\rangle\langle\psi_p^\chi|\partial_{\mathbf{k}}|\psi_s^\chi\rangle\right] \\
&= \langle\psi_s^\chi|\frac{\partial\mathcal{H}_w(\mathbf{k})}{\hbar\partial\mathbf{k}}|\psi_s^\chi\rangle + \sum_{pq}\left[\langle\psi_s^\chi|\partial_{\mathbf{k}}|\psi_p^\chi\rangle\left(\langle\psi_p^\chi|\dot{\mathbf{k}}|\psi_q^\chi\rangle\cdot\langle\psi_q^\chi|\mathbf{r}|\psi_s^\chi\rangle\right) - \left(\langle\psi_s^\chi|\mathbf{r}|\psi_p^\chi\rangle\cdot\langle\psi_p^\chi|\dot{\mathbf{k}}|\psi_q^\chi\rangle\right)\langle\psi_q^\chi|\partial_{\mathbf{k}}|\psi_s^\chi\rangle\right] \\
&= \langle\psi_s^\chi|\frac{\partial\mathcal{H}_w(\mathbf{k})}{\hbar\partial\mathbf{k}}|\psi_s^\chi\rangle + \sum_{pq}\langle\psi_p^\chi|\dot{\mathbf{k}}|\psi_q^\chi\rangle\times i\left(\langle\psi_q^\chi|\mathbf{r}|\psi_s^\chi\rangle\times\langle\psi_s^\chi|\mathbf{r}|\psi_p^\chi\rangle\right),
\end{aligned}
\tag{A1}
$$

where we have used the relations $\mathbf{r}\to i\partial_{\mathbf{k}}$ and, for $q\neq p$,

$$
\langle\psi_p^\chi|\partial_{\mathbf{k}}\mathcal{H}_w(\mathbf{k})|\psi_q^\chi\rangle = \left(\varepsilon_{\mathbf{k},q}^\chi - \varepsilon_{\mathbf{k},p}^\chi\right)\langle\psi_p^\chi|\partial_{\mathbf{k}}|\psi_q^\chi\rangle.
\tag{A2}
$$

Therefore, in the Hilbert space $\Psi = \{|\psi_+^\chi\rangle, |\psi_-^\chi\rangle\}$, we can express Eq. (A1) in the matrix form as

$$
\hat{r} = \langle\Psi|\frac{\partial\mathcal{H}_w(\mathbf{k})}{\hbar\partial\mathbf{k}}|\Psi\rangle - \begin{pmatrix} \mathrm{Tr}[\hat{\dot{k}}\times\hat{\boldsymbol{\Omega}}_+(\mathbf{k})] & 0 \\ 0 & \mathrm{Tr}[\hat{\dot{k}}\times\hat{\boldsymbol{\Omega}}_-(\mathbf{k})] \end{pmatrix} = \langle\Psi|\frac{\partial\mathcal{H}_w(\mathbf{k})}{\hbar\partial\mathbf{k}}|\Psi\rangle - \bigoplus_s\mathrm{Tr}[\hat{\dot{k}}\times\hat{\boldsymbol{\Omega}}_s(\mathbf{k})],
\tag{A3}
$$

where we denote $\hat{r} = \langle \Psi | \dot{r} | \Psi \rangle$, $\hat{\dot{k}} = \langle \Psi | \dot{k} | \Psi \rangle$, and

$$\hat{\boldsymbol{\Omega}}_s(\boldsymbol{k}) = -i \langle \Psi | \boldsymbol{r} | \psi_s^\chi \rangle \times \langle \psi_s^\chi | \boldsymbol{r} | \Psi \rangle. \tag{A4}$$

With the identities $\frac{dA}{dt} = \partial_t A + (\dot{r} \cdot \boldsymbol{\nabla}) A$ and

$$\boldsymbol{\nabla}(\dot{r} \cdot A) = \dot{r} \times (\boldsymbol{\nabla} \times A) + (\dot{r} \cdot \boldsymbol{\nabla}) A, \tag{A5}$$

we find

$$\hat{\dot{k}} = \hbar^{-1} \hat{F} = \frac{e}{\hbar} \langle \Psi | \left[\boldsymbol{\nabla} \Phi - \boldsymbol{\nabla}(\dot{r} \cdot A) + \frac{dA}{dt} \right] | \Psi \rangle$$

$$= \frac{e}{\hbar} (\boldsymbol{\nabla} \Phi + \partial_t A) - \frac{e}{\hbar} \hat{r} \times (\boldsymbol{\nabla} \times A). \tag{A6}$$

Then, Eqs. (A3) and (A6) can be expressed as Eq. (7) in the main text.

Within the adiabatic approximation, we can replace $i\partial_t \to \dot{k} \cdot r$ in the second line of Eq. (A1), which means neglecting the off-diagonal elements of $\dot{k}$, such that Eq. (A1) returns to

the conventional adiabatic pumping formula

$$\langle \psi_s^\chi(t) | \dot{r} | \psi_s^\chi(t) \rangle = \langle \psi_s^\chi | \frac{\partial \mathcal{H}_w(\boldsymbol{k})}{\hbar \partial \boldsymbol{k}} | \psi_s^\chi \rangle$$
$$- i \left[\langle \partial_{\boldsymbol{k}} \psi_s^\chi | \partial_t \psi_s^\chi \rangle - \langle \partial_t \psi_s^\chi | \partial_{\boldsymbol{k}} \psi_s^\chi \rangle \right]. \tag{A7}$$

If we neglect the off-diagonal elements of $\hat{\dot{k}}$, i.e.,

$$\langle \psi_p^\chi | \dot{k} | \psi_q^\chi \rangle = \left(\frac{e}{\hbar} \boldsymbol{\nabla} \Phi - \frac{e}{\hbar} \langle \psi_p^\chi | \dot{r} | \psi_q^\chi \rangle \times \boldsymbol{B} \right) \delta_{p,q}, \tag{A8}$$

with $\boldsymbol{\nabla} \Phi = -\boldsymbol{E} - \partial_t A$ and $\boldsymbol{B} = \boldsymbol{\nabla} \times A$, the diagonal parts of $\hat{r}$ and $\hat{\dot{k}}$ reduce to be

$$\hat{\dot{k}} = -\frac{e}{\hbar}(\boldsymbol{E} + \partial_t A) - \frac{e}{\hbar} \hat{r} \times \boldsymbol{B}, \tag{A9}$$

$$\hat{r} = \frac{\partial \mathcal{H}_{\boldsymbol{k}}}{\hbar \partial \boldsymbol{k}} + \hat{\dot{k}} \times i(\hat{r} \times \hat{r}), \tag{A10}$$

which is the conventional semiclassical equation of motion, where, for brevity, we denote $\mathcal{H}_{\boldsymbol{k}} = \operatorname{diag}(\varepsilon_{\boldsymbol{k},+}^\chi, \varepsilon_{\boldsymbol{k},-}^\chi)$ and $\hat{O} = \langle \Psi | O | \Psi \rangle$, with $O = \{r, \dot{r}, \dot{k}\}$.

In fact, the off-diagonal elements of $\hat{\dot{k}}$ will couple with the off-diagonal elements of the Berry curvature, and the resulting contribution

$$\hat{\Pi}_s^{(\text{off})}(\boldsymbol{k}, t) = \frac{e}{\hbar} \sum_{p \neq q} \frac{\varepsilon_{\boldsymbol{k},q}^\chi - \varepsilon_{\boldsymbol{k},p}^\chi}{\hbar} \left(\langle \psi_p^\chi | \boldsymbol{r} | \psi_q^\chi \rangle \times \boldsymbol{B} \right) \times \left(\langle \psi_q^\chi | \boldsymbol{r} | \psi_s^\chi \rangle \times \langle \psi_s^\chi | \boldsymbol{r} | \psi_p^\chi \rangle \right), \tag{A11}$$

with $\bar{p} = -p$, can be important to the transport. For the purpose of illustration, we turn off the electric field and provide a magnetic field $\boldsymbol{B} = B \hat{e}_z$. It is verified that the physical quantity $\hat{\boldsymbol{\Omega}}_{\boldsymbol{k}} \equiv i(\hat{r} \times \hat{r})$ equals exactly the Berry curvature

$$\hat{\Omega}_\alpha(\boldsymbol{k}) = i \epsilon_{\alpha\beta\gamma} \left\langle \frac{\partial \Psi}{\partial k_\beta} \Big| \frac{\partial \Psi}{\partial k_\gamma} \right\rangle = \frac{\chi k_\alpha}{2k^3} \begin{pmatrix} -1 & \frac{k_z}{\sqrt{k_x^2 + k_y^2}} \\ \frac{k_z}{\sqrt{k_x^2 + k_y^2}} & 1 \end{pmatrix}$$

$$= -\frac{\chi k_\alpha}{2k^3} (\eta_z - \eta_x \cot \theta). \tag{A12}$$

The diagonal part of the Berry curvature is representation independent, while the off-diagonal part relies on the representation. For example, Eq. (A12) is expressed in the σ_z representation and in the σ_x representation; the off-diagonal part changes to be $\sim \eta_x k_x / \sqrt{k_y^2 + k_z^2}$. Without the off-diagonal elements of the Berry curvature, the anomalous velocity is

$$\hat{\Pi}_{s,\alpha}^{(\text{dig})}(\boldsymbol{k}, t) = -\chi \frac{eB v_F}{2\hbar k^2} \delta_{\alpha,z} + \chi \frac{eB v_F}{2\hbar k^2} \frac{k_\alpha k_z}{k^2}, \tag{A13}$$

which is the last term in Eq. (11) in the main text. The integral of $\hat{\Pi}_{s,\alpha}^{(\text{dig})}(\boldsymbol{k}, t)$ over the momentum on a given constant-energy surface $\varepsilon_{\boldsymbol{k},s}^\chi = \epsilon$ will contribute a pumping current density

$$j_{P,\alpha}^\chi = -e \int \frac{d^3 \boldsymbol{k}}{(2\pi)^3} \hat{\Pi}_{s,\alpha}^{(\text{dig})}(\boldsymbol{k}, t) \delta(\epsilon - \varepsilon_{\boldsymbol{k},s}^\chi) = \frac{2}{3} \chi \frac{e^2}{h^2} B \delta_{\alpha,z}. \tag{A14}$$

If we include the off-diagonal contribution, the anomalous velocity becomes

$$\hat{\boldsymbol{\Pi}}_s(\boldsymbol{k}, t) = \hat{\boldsymbol{\Pi}}_s^{(\text{dig})}(\boldsymbol{k}, t) + \hat{\boldsymbol{\Pi}}_s^{(\text{off})}(\boldsymbol{k}, t)$$

$$= \chi \frac{eB v_F}{2\hbar k^2} \left(1 + s\chi \frac{k_z}{k} \right) \left(\frac{k_x k_z}{k_x^2 + k_y^2}, \frac{k_y k_z}{k_x^2 + k_y^2}, -1 \right). \tag{A15}$$

Then, the pumping current density for each constant-energy surface

$$j_{P,\alpha}^\chi = -e \int \frac{d^3 \boldsymbol{k}}{(2\pi)^3} \hat{\Pi}_{s,\alpha}(\boldsymbol{k}, t) \delta(\epsilon - \varepsilon_{\boldsymbol{k},s}^\chi) = \chi \frac{e^2}{h^2} B \delta_{\alpha,z} \tag{A16}$$

will be quantized exactly to the chirality χ of the Weyl node, which characterizes the topological nature of the system more robustly.

APPENDIX B: DISCUSSION OF THE CHIRAL CHANNELS AND SEMICLASSICAL QUANTIZATION OF THE WAVE VECTOR

Upon application of the magnetic field, the wave vector, according to the Peierls substitution, turns out to be

$$\boldsymbol{k} \to \boldsymbol{\kappa} = \boldsymbol{k} + \frac{e}{\hbar} A, \tag{B1}$$

and the system Hamiltonian becomes $\mathcal{H}_w(\kappa_x, \kappa_y, \kappa_z)$. It is easy to verify the commutation relation

$$\boldsymbol{\kappa} \times \boldsymbol{\kappa} = -i \frac{e}{\hbar} (\boldsymbol{\nabla} \times A). \tag{B2}$$

As a consequence, for $\boldsymbol{B} = B\hat{e}_z$, κ_x and κ_y are noncommutable, i.e.,

$$[\kappa_x, \kappa_y] = -i\frac{eB}{\hbar} = -\frac{i}{\ell_B^2}, \tag{B3}$$

with $\ell_B = \sqrt{\hbar/eB}$ being the magnetic length. Then, let us consider the eigenvalue problem $\mathcal{H}_w(\kappa_x, \kappa_y, k_z)\psi = E\psi$, namely,

$$\chi\hbar\upsilon_F \begin{pmatrix} k_z & \kappa_x - i\kappa_y \\ \kappa_x + i\kappa_y & -k_z \end{pmatrix}\begin{pmatrix} a \\ b \end{pmatrix} = E\begin{pmatrix} a \\ b \end{pmatrix}, \tag{B4}$$

from which we can obtain

$$\left(\kappa_x^2 + \kappa_y^2 + i[\kappa_x, \kappa_y]\right)a = \left(\frac{E^2}{\hbar^2\upsilon_F^2} - \kappa_z^2\right)a, \tag{B5a}$$

$$\left(\kappa_x^2 + \kappa_y^2 - i[\kappa_x, \kappa_y]\right)b = \left(\frac{E^2}{\hbar^2\upsilon_F^2} - \kappa_z^2\right)b. \tag{B5b}$$

These two equations cannot be satisfied simultaneously unless $[\kappa_x, \kappa_y] = 0$. For $\kappa_x^2 + \kappa_y^2 \gg 1/\ell_B^2$, we may regard κ_x and κ_y as commutable, such that the eigenvalue problem can be solved approximately as $\tilde{\Psi} = \{|\tilde{\psi}_+^\chi\rangle, |\tilde{\psi}_-^\chi\rangle\}$, where

$$|\tilde{\psi}_s^\chi\rangle = \frac{1}{A}\begin{pmatrix} \kappa_x - i\kappa_y \\ s\chi\sqrt{\kappa_x^2 + \kappa_y^2 + \kappa_z^2} - \kappa_z \end{pmatrix}, \tag{B6}$$

with A being the normalized coefficient. Then, we can define the Berry curvature as usual in the parameter space $(\kappa_x, \kappa_y, \kappa_z)$, i.e.,

$$\tilde{\Omega}_\alpha(\boldsymbol{k}) = i\epsilon_{\alpha\beta\gamma}\left\langle \frac{\partial\tilde{\Psi}}{\partial\kappa_\beta}\middle|\frac{\partial\tilde{\Psi}}{\partial\kappa_\gamma}\right\rangle, \tag{B7}$$

which can be obtained from Eq. (A12) with the replacement $\boldsymbol{k} \to \boldsymbol{\kappa}$. However, as $\kappa_x^2 + \kappa_y^2 \sim 1/\ell_B^2$, especially for the limiting case $\kappa_x^2 + \kappa_y^2 \to 0$, the contradiction between the two equations in Eq. (B5) becomes irreconcilable.

To resolve the conflict, we should quantize $\kappa_{x,y}$ by the Sommerfeld quantization condition

$$\oint \boldsymbol{p} \cdot d\boldsymbol{r} = \left(n + \frac{1}{2}\right)h. \tag{B8}$$

We first introduce the quasicoordinates $\xi_x = \ell_B^2\kappa_y$ and $\xi_y = -\ell_B^2\kappa_x$, according to the commutation relation between the coordinate and wave vector $[x, k_x] = i$. Then, we perform the quantization

$$\oint \kappa_x d\xi_x = \ell_B^2\oint \kappa_x d\kappa_y = 2\pi\left(n + \frac{1}{2}\right) \quad (n = 1, 2, 3, \dots), \tag{B9}$$

which leads to

$$\kappa_x^2 + \kappa_y^2 = \frac{2n+1}{\ell_B^2}. \tag{B10}$$

Therefore, Eq. (B5) can be expressed as

$$\left(\kappa_x^2 + \kappa_y^2\right)\phi_m = \left(\frac{E^2}{\hbar^2\upsilon_F^2} - \kappa_z^2 - \frac{1}{\ell_B^2}\right)\phi_m, \tag{B11a}$$

$$\left(\kappa_x^2 + \kappa_y^2\right)\phi_n = \left(\frac{E^2}{\hbar^2\upsilon_F^2} - \kappa_z^2 + \frac{1}{\ell_B^2}\right)\phi_n, \tag{B11b}$$

where $\phi_{m,n}$ is the eigenfunction of $\kappa_x^2 + \kappa_y^2$. Consequently, if $n = m + 1$, the two equations in Eq. (B5) can be satisfied simultaneously. After that, the energy can be solved to be

$$\begin{aligned}\varepsilon_{n\geqslant 1,s}^\chi(k_z) &= s\hbar\upsilon_F\sqrt{\kappa_x^2 + \kappa_y^2 + \kappa_z^2 - 1/\ell_B^2} \\ &= s\hbar\upsilon_F\sqrt{\frac{2n}{\ell_B^2} + k_z^2}, \end{aligned} \tag{B12}$$

which becomes the achiral Landau levels. Additionally, for $\kappa_x^2 + \kappa_y^2 = 0$, we can find another solution,

$$a = 0, \quad \frac{E^2}{\hbar^2\upsilon_F^2} - k_z^2 = 0, \tag{B13}$$

to Eq. (B5), which, according to Eq. (B4), gives a chirality-dependent energy level

$$\varepsilon_0^\chi(k_z) = -\chi\hbar\upsilon_F k_z, \tag{B14}$$

corresponding to the wave function

$$|\tilde{\psi}_0^\chi\rangle = \begin{pmatrix} 0 \\ 1 \end{pmatrix}. \tag{B15}$$

Therefore, as the magnetic field is turned on, the spectrum will be separated into two parts: a part with achiral dispersion $\varepsilon_{\boldsymbol{k},s}^\chi \simeq s\hbar\upsilon_F\sqrt{k_x^2 + k_y^2 + k_z^2}$ which maintains the shape of the Weyl cone and possesses chirality-dependent Berry curvature and a part with chiral dispersion $\varepsilon_0^\chi(k_z) = -\chi\hbar\upsilon_F k_z$ but without Berry curvature. Consequently, the achiral dispersion, i.e., the Weyl cone, acquires an anomalous velocity at each $\boldsymbol{k}$ point, as if it were decorated with chiral channels, as plotted in Figs. 1(a)–1(c).

[1] M. Z. Hasan and C. L. Kane, Rev. Mod. Phys. **82**, 3045 (2010).

[2] X.-L. Qi and S.-C. Zhang, Rev. Mod. Phys. **83**, 1057 (2011).

[3] M. Z. Hasan, S.-Y. Xu, I. Belopolski, and S.-M. Huang, Annu. Rev. Condens. Matter Phys. **8**, 289 (2017).

[4] B. Yan and C. Felser, Annu. Rev. Condens. Matter Phys. **8**, 337 (2017).

[5] N. P. Armitage, E. J. Mele, and A. Vishwanath, Rev. Mod. Phys. **90**, 015001 (2018).

[6] D.-W. Zhang, Y.-Q. Zhu, Y. X. Zhao, H. Yan, and S.-L. Zhu, Adv. Phys. **67**, 253 (2018).

[7] X. Wan, A. M. Turner, A. Vishwanath, and S. Y. Savrasov, Phys. Rev. B **83**, 205101 (2011).

[8] K.-Y. Yang, Y.-M. Lu, and Y. Ran, Phys. Rev. B **84**, 075129 (2011).

[9] Z. Wang, Y. Sun, X.-Q. Chen, C. Franchini, G. Xu, H. Weng, X. Dai, and Z. Fang, Phys. Rev. B **85**, 195320 (2012).

[10] Z. Wang, H. Weng, Q. Wu, X. Dai, and Z. Fang, Phys. Rev. B **88**, 125427 (2013).

[11] G. Xu, H. Weng, Z. Wang, X. Dai, and Z. Fang, Phys. Rev. Lett. **107**, 186806 (2011).

[12] S. M. Young, S. Zaheer, J. C. Y. Teo, C. L. Kane, E. J. Mele, and A. M. Rappe, Phys. Rev. Lett. **108**, 140405 (2012).

[13] A. A. Burkov, Phys. Rev. Lett. **113**, 247203 (2014).

[14] S. Nandy, G. Sharma, A. Taraphder, and S. Tewari, Phys. Rev. Lett. **119**, 176804 (2017).

[15] C. M. Wang, H.-Z. Lu, and S.-Q. Shen, Phys. Rev. Lett. **117**, 077201 (2016).

[16] X.-S. Li, C. Wang, M.-X. Deng, H.-J. Duan, P.-H. Fu, R.-Q. Wang, L. Sheng, and D. Y. Xing, Phys. Rev. Lett. **123**, 206601 (2019).

[17] A. A. Taskin, H. F. Legg, F. Yang, S. Sasaki, Y. Kanai, K. Matsumoto, A. Rosch, and Y. Ando, Nat. Commun. **8**, 1340 (2017).

[18] M.-X. Deng, J.-Y. Ba, R. Ma, W. Luo, R.-Q. Wang, L. Sheng, and D. Y. Xing, Phys. Rev. Research **2**, 033346 (2020).

[19] M.-X. Deng, G. Y. Qi, R. Ma, R. Shen, R.-Q. Wang, L. Sheng, and D. Y. Xing, Phys. Rev. Lett. **122**, 036601 (2019).

[20] D. T. Son and B. Z. Spivak, Phys. Rev. B **88**, 104412 (2013).

[21] K.-S. Kim, H.-J. Kim, and M. Sasaki, Phys. Rev. B **89**, 195137 (2014).

[22] A. A. Burkov, Phys. Rev. B **91**, 245157 (2015).

[23] V. A. Zyuzin, Phys. Rev. B **95**, 245128 (2017).

[24] M.-X. Deng, W. Luo, R.-Q. Wang, L. Sheng, and D. Y. Xing, Phys. Rev. B **96**, 155141 (2017).

[25] K. Das and A. Agarwal, Phys. Rev. B **99**, 085405 (2019).

[26] M.-X. Deng, H.-J. Duan, W. Luo, W. Y. Deng, R.-Q. Wang, and L. Sheng, Phys. Rev. B **99**, 165146 (2019).

[27] D. Ma, H. Jiang, H. Liu, and X. C. Xie, Phys. Rev. B **99**, 115121 (2019).

[28] M.-X. Deng, Y.-Y. Yang, W. Luo, R. Ma, C.-Y. Zhu, R.-Q. Wang, L. Sheng, and D. Y. Xing, Phys. Rev. B **100**, 235105 (2019).

[29] S.-H. Zheng, H.-J. Duan, J.-K. Wang, J.-Y. Li, M.-X. Deng, and R.-Q. Wang, Phys. Rev. B **101**, 041408(R) (2020).

[30] Y.-Y. Yang, M.-X. Deng, H.-J. Duan, W. Luo, and R.-Q. Wang, Phys. Rev. B **101**, 205137 (2020).

[31] S. Ghosh, D. Sinha, S. Nandy, and A. Taraphder, Phys. Rev. B **102**, 121105(R) (2020).

[32] Y.-H. Lei, Y.-L. Zhou, H.-J. Duan, M.-X. Deng, Z.-E. Lu, and R.-Q. Wang, Phys. Rev. B **104**, L121117 (2021).

[33] M. Yang, Q.-T. Hou, and R.-Q. Wang, New J. Phys. **21**, 113057 (2019).

[34] M. Yang, Q.-T. Hou, and R.-Q. Wang, New J. Phys. **22**, 033015 (2020).

[35] D.-W. Zhang, S.-L. Zhu, and Z. D. Wang, Phys. Rev. A **92**, 013632 (2015).

[36] Z. K. Liu, B. Zhou, Y. Zhang, Z. J. Wang, H. M. Weng, D. Prabhakaran, S.-K. Mo, Z. X. Shen, Z. Fang, X. Dai, Z. Hussain, and Y. L. Chen, Science **343**, 864 (2014).

[37] M. Neupane, S.-Y. Xu, R. Sankar, N. Alidoust, G. Bian, C. Liu, I. Belopolski, T.-R. Chang, H.-T. Jeng, H. Lin, A. Bansil, F. Chou, and M. Z. Hasan, Nat. Commun. **5**, 3786 (2014).

[38] S.-Y. Xu et al., Science **349**, 613 (2015).

[39] B. Q. Lv, N. Xu, H. M. Weng, J. Z. Ma, P. Richard, X. C. Huang, L. X. Zhao, G. F. Chen, C. E. Matt, F. Bisti, V. N. Strocov, J.

[40] Mesot, Z. Fang, X. Dai, T. Qian, M. Shi, and H. Ding, Nat. Phys. **11**, 724 (2015).

[40] B. Q. Lv, H. M. Weng, B. B. Fu, X. P. Wang, H. Miao, J. Ma, P. Richard, X. C. Huang, L. X. Zhao, G. F. Chen, Z. Fang, X. Dai, T. Qian, and H. Ding, Phys. Rev. X **5**, 031013 (2015).

[41] L. Lu, Z. Wang, D. Ye, L. Ran, L. Fu, J. D. Joannopoulos, and M. Soljačić, Science **349**, 622 (2015).

[42] D. Rees, K. Manna, B. Lu, T. Morimoto, H. Borrmann, C. Felser, J. E. Moore, D. H. Torchinsky, and J. Orenstein, Sci. Adv. **6**, eaba0509 (2020).

[43] N. Morali, R. Batabyal, P. Kumar-Nag, N. Avraham, H. Beidenkopf, P. Vir, E. Liu, C. Shekhar, C. Felser, T. Hughes, and V. Madhavan, Nat. Commun. **12**, 4269 (2021).

[44] L. Luo, H.-X. Wang, Z.-K. Lin, B. Jiang, Y. Wu, F. Li, and J.-H. Jiang, Nat. Mater. **20**, 794 (2021).

[45] G. B. Osterhoudt, Y. Wang, C. A. C. Garcia, V. M. Plisson, J. Gooth, C. Felser, P. Narang, and K. S. Burch, Phys. Rev. X **11**, 011017 (2021).

[46] D. Kumar, C.-H. Hsu, R. Sharma, T.-R. Chang, P. Yu, J. Wang, G. Eda, G. Liang, and H. Yang, Nat. Nanotechnol. **16**, 421 (2021).

[47] P. Puphal, V. Pomjakushin, N. Kanazawa, V. Ukleev, D. J. Gawryluk, J. Ma, M. Naamneh, N. C. Plumb, L. Keller, R. Cubitt, E. Pomjakushina, and J. S. White, Phys. Rev. Lett. **124**, 017202 (2020).

[48] X. Yuan, C. Zhang, Y. Zhang, Z. Yan, T. Lyu, M. Zhang, Z. Li, C. Song, M. Zhao, P. Leng, M. Ozerov, X. Chen, N. Wang, Y. Shi, H. Yan, and F. Xiu, Nat. Commun. **11**, 1259 (2020).

[49] B. Zhao, D. Khokhriakov, Y. Zhang, H. Fu, B. Karpiak, A. M. Hoque, X. Xu, Y. Jiang, B. Yan, and S. P. Dash, Phys. Rev. Research **2**, 013286 (2020).

[50] Z.-Y. Wang, X.-C. Cheng, B.-Z. Wang, J.-Y. Zhang, Y.-H. Lu, C.-R. Yi, S. Niu, Y. Deng, X.-J. Liu, S. Chen, and J.-W. Pan, Science **372**, 271 (2021).

[51] M. E. Peskin and D. V. Schroeder, *An Introduction to Quantum Field Theory* (Westview, Boulder, CO, 1995).

[52] H. Nielsen and M. Ninomiya, Phys. Lett. B **130**, 389 (1983).

[53] G. E. Volovik, *The Universe in a Helium Droplet* (Oxford University Press, Oxford, 2003).

[54] S.-M. Huang, S.-Y. Xu, I. Belopolski, C.-C. Lee, G. Chang, B. Wang, N. Alidoust, G. Bian, M. Neupane, C. Zhang, S. Jia, A. Bansil, H. Lin, and M. Z. Hasan, Nat. Commun. **6,** 7373 (2015).

[55] H. Weng, C. Fang, Z. Fang, B. A. Bernevig, and X. Dai, Phys. Rev. X **5**, 011029 (2015).

[56] L. X. Yang, Z. K. Liu, Y. Sun, H. Peng, H. F. Yang, T. Zhang, B. Zhou, Y. Zhang, Y. F. Guo, M. Rahn, D. Prabhakaran, Z. Hussain, S.-K. Mo, C. Felser, B. Yan, and Y. L. Chen, Nat. Phys. **11**, 728 (2015).

[57] J. Xiong, S. K. Kushwaha, T. Liang, J. W. Krizan, M. Hirschberger, W. Wang, R. J. Cava, and N. P. Ong, Science **350**, 413 (2015).

[58] C.-Z. Li, L.-X. Wang, H. Liu, J. Wang, Z.-M. Liao, and D.-P. Yu, Nat. Commun. **6**, 10137 (2015).

[59] Y. Wang, E. Liu, H. Liu, Y. Pan, L. Zhang, J. Zeng, Y. Fu, M. Wang, K. Xu, Z. Huang, Z. Wang, H.-Z. Lu, D. Xing, B. Wang, X. Wan, and F. Miao, Nat. Commun. **7**, 13142 (2016).

[60] Y.-Y. Lv, X. Li, B.-B. Zhang, W. Y. Deng, S.-H. Yao, Y. B. Chen, J. Zhou, S.-T. Zhang, M.-H. Lu, L. Zhang, M. Tian, L. Sheng, and Y.-F. Chen, Phys. Rev. Lett. **118**, 096603 (2017).

[61] P. Goswami and S. Tewari, Phys. Rev. B **88**, 245107 (2013).

[62] K. Fujikawa, Phys. Rev. D **21**, 2848 (1980).

[63] A. A. Zyuzin and A. A. Burkov, Phys. Rev. B **86**, 115133 (2012).

[64] C. Rylands, A. Parhizkar, A. A. Burkov, and V. Galitski, Phys. Rev. Lett. **126**, 185303 (2021).

[65] D. Xiao, M.-C. Chang, and Q. Niu, Rev. Mod. Phys. **82**, 1959 (2010).

[66] M. N. Ali, J. Xiong, S. Flynn, J. Tao, Q. D. Gibson, L. M. Schoop, T. Liang, N. Haldolaarachchige, M. Hirschberger, N. Ong, and R. Cava, Nature (London) **514**, 205 (2014).

[67] C. Shekhar, A. K. Nayak, Y. Sun, M. Schmidt, M. Nicklas, I. Leermakers, U. Zeitler, Y. Skourski, J. Wosnitza, Z. Liu, Y. Chen, W. Schnelle, H. Borrmann, Y. Grin, C. Felser, and B. Yan, Nat. Phys. **11**, 645 (2015).

[68] S. A. Parameswaran, T. Grover, D. A. Abanin, D. A. Pesin, and A. Vishwanath, Phys. Rev. X **4**, 031035 (2014).

[69] J. Chen, T. Zhang, J. Wang, N. Zhang, W. Ji, S. Zhou, and Y. Chai, Adv. Funct. Mater. **31**, 2104192 (2021).

[70] L. Chen and K. Chang, Phys. Rev. Lett. **125**, 047402 (2020).

[71] N. P. Ong and S. Liang, Nat. Rev. Phys. **3**, 394 (2021).

[72] W. Luo, M.-X. Deng, W. Y. Deng, and L. Sheng, J. Phys.: Condens. Matter **31**, 125502 (2019).

[73] L. Privitera, A. Russomanno, R. Citro, and G. E. Santoro, Phys. Rev. Lett. **120**, 106601 (2018).

[74] M. I. N. Rosa, R. K. Pal, J. R. F. Arruda, and M. Ruzzene, Phys. Rev. Lett. **123**, 034301 (2019).

[75] Y. Xia, E. Riva, M. I. N. Rosa, G. Cazzulani, A. Erturk, F. Braghin, and M. Ruzzene, Phys. Rev. Lett. **126**, 095501 (2021).

[76] H. Goldstein, C. Poole, and J. Safko, *Classical Mechanics* (American Association of Physics Teachers, 2002).

[77] C.-L. Zhang, Z. Yuan, Q.-D. Jiang, B. Tong, C. Zhang, X. C. Xie, and S. Jia, Phys. Rev. B **95**, 085202 (2017).

[78] C.-K. Chan, N. H. Lindner, G. Refael, and P. A. Lee, Phys. Rev. B **95**, 041104(R) (2017).

[79] K. Taguchi, T. Imaeda, M. Sato, and Y. Tanaka, Phys. Rev. B **93**, 201202(R) (2016).